JCTC Journal of Chemical Theory and Computation

ARTICLE

pubs.acs.org/JCTC

Coupled Cluster in Condensed Phase. Part II: Liquid Hydrogen Fluoride from Quantum Cluster Equilibrium Theory

Christian Spickermann,[†,§] Eva Perlt,[†] Michael von Domaros,[†] Martin Roatsch,[†] Joachim Friedrich,[‡] and Barbara Kirchner*[,†]

[†]Wilhelm-Ostwald-Institut für Physikalische und Theoretische Chemie, Universität Leipzig, Linnéstrasse 2, D-04103 Leipzig, Germany

[‡]Institute for Chemistry, Chemnitz University of Technology, Strasse der Nationen 62, 09111 Chemnitz, Germany

ABSTRACT: Treating the bulk phase with high-level ab initio methods, such as coupled cluster, is a nontrivial task because of the computational costs of these electronic structure methods. In this part of our hydrogen fluoride study we make use of the quantum cluster equilibrium method, which employs electronic structure input of small clusters and combines it with simple statistical mechanics in order to describe condensed phase phenomena. If no parameter adjustment is applied, then the lower quantum chemical methods, such as density functional theory in conjunction with the generalized gradient approximation, provide wrong results in accordance with the description of the strength of the interaction in the clusters. While density functional theory describes the liquid phase too dense due to overbinding of the clusters, the coupled cluster method and the perturbation theory at the complete basis set limit agree well with experimental observations. If we allow the two parameters in the quantum cluster equilibrium method to vary, then these are able to compensate the overbinding, thereby leading to very good agreement with experiment. Correlated methods in combination with small basis sets giving rise to too weakly bound clusters cannot reach this accuracy even if the parameters are flexible. Only at the complete basis set limit, the performance of the correlated methods is again excellent.

1. INTRODUCTION

Liquid hydrogen fluoride (HF) is a substance of importance for the chemical industry as well as academic research, e.g., its superacidic properties have been successfully employed for the investigation and clarification of reaction mechanisms.[1−3] However, the structural as well as thermodynamic data available for liquid HF in literature has been rather scarce, which is not surprising considering the highly toxic and corrosive properties of this fluid. Indeed, it has been proposed to rather calculate its properties than to measure them.[4,5] However, the accurate treatment of the liquid state in terms of computational chemistry is still a nontrivial task. The most obvious choice for the modeling of condensed systems lies in traditional molecular dynamics simulations, which account for the intermolecular interactions being important at high densities in terms of analytical potential functions fitted to reproduce macroscopic experimental data. Although long simulation times and large sample sizes can be realized in terms of this approach, the quantum mechanical character of the molecular system is most often completely neglected and effects, like cooperativity or spontaneous events, fall outside the reach of these kind of calculations. Ab initio molecular dynamics simulations can account for these deficiencies, but due to the large computational effort, simulation time as well as sample size are restricted considerably in these models, which makes the prediction of thermodynamical quantities very difficult for systems exhibiting many degrees of freedom. The quantum cluster equilibrium (QCE) theory[6] circumvents the computational time bottleneck, i.e., these sampling problems, by modeling the liquid phase as a thermodynamic equilibrium of distinct cluster structures, for which an approximate but analytical partition function and thus a gateway to the thermodynamics of the condensed phase is available. Furthermore, the introduction of highly accurate post-Hartree−Fock electronic structure data, such as the coupled cluster method, is possible.

In cases of highly associated liquids, numerous successful applications of the QCE model in this field were demonstrated.[7−21] However, liquid HF as one of the most generic associated systems has not been in the focus of the QCE approach so far, although there are several other computational studies dealing with this substance in literature.[22−34] Most computational approaches toward HF in terms of static ab initio methods were mainly concerned with cooperative effects in isolated cluster structures,[22−29] but several traditional as well as ab initio molecular dynamics studies on liquid HF have also been published, which mainly deal with structural aspects of the fluid phase.[30−34]

Ab initio molecular dynamics simulations[31,34] indicate a predominance of chain-like structures in liquid HF at ambient as well as supercritical states. In contrast, experimental studies do not definitely attest this observation but rather assume an equality between the structure of the solid (parallel zigzag chains) and the structure of the liquid.[35] This is also true in case of the elevated temperature regime, for which structural changes of the hydrogen-bonded species are indicated, but no prediction about the kind of these changes could be made.[35] Furthermore, important electron correlation effects have been neglected in these studies so far. Earlier experimental investigations also explicitly discuss the occurrence of cyclic species in the liquid phase and highlight that cooperative effects, which are assumed to play only a minor role in the liquid, could as well seriously affect the liquid phase structures of strongly associated liquids, such as water or HF.[36]

The purpose of this article is to apply the coupled cluster method to the liquid phase of HF via the QCE approach. To the best of our

Received: January 31, 2011
Published: March 16, 2011

knowledge, the coupled cluster method has never been combined with the QCE approach. It has been used to derive ab initio force field parameters,[37] but it has not been used directly in condensed phase calculations.

The article is organized as follows. A short introduction to the QCE method is given in the next section, Section 2. After this, the investigated structures are presented and the appropriate binding energies are discussed. In Section 3, the results for the liquid phase are presented, and the influence of the electronic structure method is investigated. Finally, the behavior at the phase transition is presented.

2. THEORY

2.1. Quantum Cluster Equilibrium (QCE) Method. A full derivation of the QCE theory can be found elsewhere,[8,9,13,38] with the most detailed description in refs 9 and 13. As laid out in these references, the basic idea of the QCE model is a thermodynamic equilibrium between different sized clusters and one corresponding reference monomer. The equilibrium equation thus reads

$$C_1 \leftrightarrows \frac{C_2}{i(2)} \leftrightarrows \ ... \leftrightarrows \frac{C_{\mathscr{P}}}{i(\mathscr{P})} \leftrightarrows \ ... \leftrightarrows \frac{C_\eta}{i(\eta)} \tag{1}$$

Here $C_{\mathscr{P}}$ denotes a cluster of $i(\mathscr{P})$ monomer units up to $i(\eta)$ monomer units forming the largest cluster, and η represents the total number of clusters considered in the mixture. Using the relation between the molecular partition function $q_{\mathscr{P}}$ of the particle $\mathscr{P}$ and the chemical potential $\mu_{\mathscr{P}}$ for which the same equilibrium holds, as in eq 1:

$$\mu_{\mathscr{P}} = -kT \ln\left(\frac{q_{\mathscr{P}}}{N_{\mathscr{P}}}\right) \tag{2}$$

followed by application of the particle conservation

$$N_A = N_1 + i(2)N_2 + \ ... + i(\mathscr{P})N_{\mathscr{P}} + \ ... + i(\eta)N_\eta \tag{3}$$

leads to the crucial step of the QCE calculation, i.e., an iterative cycle for the root finding of the population polynomial and the volume polynomial. Here k denotes the Boltzmann constant, T the temperature, N_A the Avogadro number, and $N_{\mathscr{P}}$ the particle number of particle $\mathscr{P}$. Using moles $n_{\mathscr{P}}$=$N_{\mathscr{P}}/N_A$ instead of particle numbers, the population polynomial for the monomer as reference species is given by the following expression:

$$0 = -1 + \sum_{\mathscr{P}=1}^{\eta} \left[\frac{i(\mathscr{P}) q_{\mathscr{P}} N_A^{i(\mathscr{P})-1}}{q_1^{i(\mathscr{P})}}\right] n_1^{i(\mathscr{P})} \tag{4}$$

If there are cluster sizes which do not exist in the chosen cluster mixture, then the vanishing partition function $q_{\mathscr{P}}$ for this particular $i(\mathscr{P})$ value will ensure the correct form of the polynomial. The populations of all other clusters are completely determined in terms of the monomer population[6,8] and allow the calculation of the canonical QCE partition function Q^{tot} according to

$$Q^{tot} = \prod_{\mathscr{P}=1}^{\eta} Q_{\mathscr{P}}(\{N_{\mathscr{P}}\}, V, T) = \prod_{\mathscr{P}=1}^{\eta} \frac{q_{\mathscr{P}}^{N_{\mathscr{P}}}}{N_{\mathscr{P}}!} \tag{5}$$

The molecular partition function $q_{\mathscr{P}}$ may be decomposed into its molecular degrees of freedom assuming that those are independent of each other

$$q_{\mathscr{P}} = q_{\mathscr{P}}^{tr} \cdot q_{\mathscr{P}}^{rot} \cdot q_{\mathscr{P}}^{vib} \cdot q_{\mathscr{P}}^{el} \tag{6}$$

with the superscripts denoting translational, rotational, vibrational, and electronic contributions, respectively. By employing the relationship between pressure p and the partition function Q^{tot}, a third-order polynomial for the phase volume V can be derived, yielding

$$0 = -pV^3 + \left[kT \sum_{\mathscr{P}=1}^{\eta} N_{\mathscr{P}} + pV_{excl}\right] V^2 - \left[\sum_{\mathscr{P}=1}^{\eta} N_{\mathscr{P}} i(\mathscr{P}) a_{mf}\right] V + \left[\sum_{\mathscr{P}=1}^{\eta} N_{\mathscr{P}} i(\mathscr{P}) a_{mf}\right] V_{excl} \tag{7}$$

In this equation V_{excl} denotes an excluded volume term according to the population-weighted sum of the cluster volumes and a_{mf} an empirical cluster−cluster interaction parameter described in the following.

In order to treat interactions between clusters (intercluster interaction), a van der Waals-like meanfield term of the form

$$u_{\mathscr{P}}^{int} = u_{\mathscr{P}}^{int}(i(\mathscr{P}), V) = -a_{mf} \frac{i(\mathscr{P})}{V} \tag{8}$$

was suggested, with a_{mf} being a substance-specific scaling factor, and V the overall phase volume as obtained from the volume polynomial (eq 7).[6] The energy term entering the electronic cluster partition function $q_{\mathscr{P}}^{el}$ is thus given as the sum of the intracluster and intercluster interactions, and $q_{\mathscr{P}}^{el}$ is obtained from

$$q_{\mathscr{P}}^{el} = \exp(-[E_{\mathscr{P}}^{intra} + u_{\mathscr{P}}^{int}]/kT) \tag{9}$$

where $E_{\mathscr{P}}^{intra}$ denotes the adiabatic intracluster interaction energy according to

$$E_{\mathscr{P}}^{intra} = E_{\mathscr{P}} - i(\mathscr{P})E_1 \tag{10}$$

Please note that besides a_{mf} the model depends on another parameter (b_{xv}). It scales the cluster volume estimates according to the sum of van der Waals spheres so that it can be excluded for

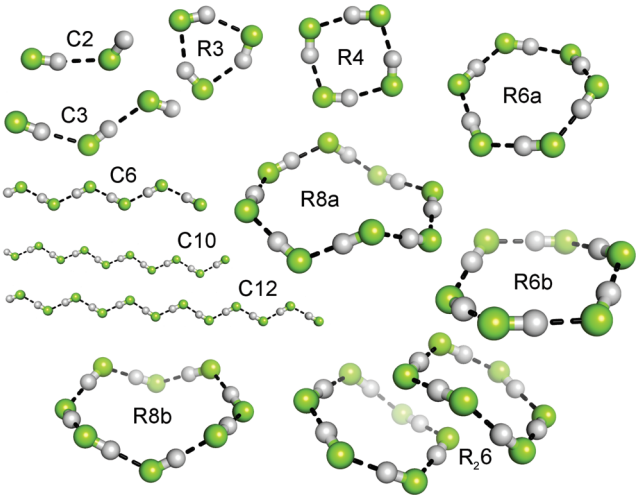

Figure 1. Ball-and-stick model of the investigated clusters as obtained by MP2/TZVP calculations. C denotes chain structures whereas R denotes cyclic structures. The R_26 cluster is built up of two stacked six-membered rings.

Table 1. Adiabatic Interaction Energies $E^{\text{intra}}_{\mathscr{P}}$ According to eq 10 for All Investigated Clusters and Different Electronic Structure Methods[a]

		CCSD(T)	MP2				B-P86	PBE
cluster	$i(\mathscr{P})$	CBS	CBS	QZVP*	QZVP	TZVP	TZVP	TZVP
C2	2	−19.48	−19.19	−18.73	−18.73	−18.54	−19.23	−22.92
C3	3	−45.13	−44.60	−43.58	−43.57	−42.98	−45.74	−53.13
R3	3	−65.12	−63.99	−62.06	−62.06	−56.80	−69.38	−78.39
R4	4	−119.01	−118.43	−115.12	−115.12	−106.36	−131.97	−145.17
C6	6	–	–	–	–	−129.88	−145.05	−163.15
R6a	6	−198.72	−198.85	−193.09	−193.04	−183.78	−223.57	−244.80
R6b	6	−199.05	−199.19	−193.41	−193.41	−183.95	−224.34	−245.55
R8a	8	−268.81	−269.00	−261.30	−260.82	−250.46	−303.98	−331.77
R8b	8	−269.11	−269.40	−261.92	−261.81	−250.84	−305.27	−333.54
C10	10	–	–	–	–	−254.41	–	–
C12	12	–	–	–	–	−317.70	−368.30	–
R_26	12	−415.07	−412.41	−397.82	−397.82	−375.71	−447.04	−499.42

[a] All energies in kJ/mol. Some results are missing because the corresponding geometries are no minimum structures.

translation.[8] Both parameters a_{mf} and b_{xv} are determined by a parameter optimization technique (PO) which works as follows: Different combinations of values for a_{mf} and b_{xv} enter a QCE calculation yielding different isobars $V_c(T)$. For each of these isobars an error norm $\|\Delta V\|$ with respect to an experimental reference isobar $V_r(T)$ is determined according to

$$\| \Delta V \| = \sqrt{\sum_T (V_c(T) - V_r(T))^2} \qquad (11)$$

with the summation running over all temperatures. The combination resulting in the lowest error norm is taken to be most reliable.[18]

In order to investigate the impact of certain clusters or cluster motifs on the liquid phase and to identify destabilizing structures, a cluster set optimization procedure (CSO) is additionally carried out, i.e., clusters giving populations below a certain threshold value over the whole temperature range are systematically left out and taken into account, and thereby for each permutation, a new cluster set is obtained. For each of these sets a parameter optimization is carried out. Finally, the cluster set together with its optimized parameters that yields the lowest error norm is taken to be the best result.

The QCE calculations were performed employing our own software, i.e., the PEACEMAKER code.[38] This code is freely available from http://www.uni-leipzig.de/~peacemaker/.

3. RESULTS

In order to perform QCE calculations we need a set of clusters with characteristic topologies similar to a basis set in quantum chemical calculations. The clusters building up the set should represent certain motifs of the investigated phase rather than portray the phase in analogy to a complete basis set in quantum chemistry. In case of HF we chose different sized ring and chain structures. Furthermore we included the R_26 cluster which consists of two stacked ring structures. Figure 1 shows all clusters from which certain examples were used as input in the following QCE calculations.

3.1. Interaction Energies. The interaction energies which enter eq 10 for the different clusters are calculated with different electronic structure methods, see table 1. Computational details can be found in ref 39. Concerning the basis set superposition error, ref 40 shows that the CP-corrected energies converge from above to the complete basis set limit, whereas the noncorrected values converge from below to the complete basis set limit with increasing basis sets. Therefore, the energies applied to the QCE calculations are the averaged values of CP-corrected and uncorrected energy.

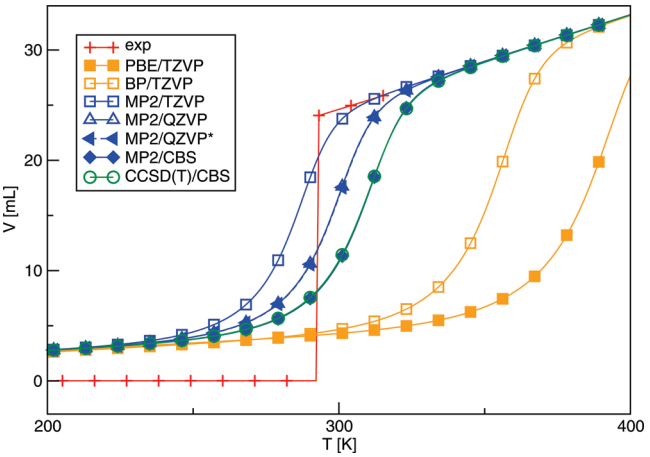

Figure 2. Isobars from different quantum chemical methods without adjusting the parameters, i.e., the $\text{QCE}^{(0)}$ model.

As one can see from Table 1, energies as obtained by the density functional theory (DFT) approaches are smaller, and thus clusters are suggested to be more stable than those obtained by the MP2 and the CCSD(T) approach. Regarding the MP2 calculations, one observes a strong basis set dependence with slightly increasing stability of the clusters when enlarging the basis set applied. A similar trend is observed when improving the level of theory from MP2 to CCSD(T) except for the six- and eight-membered rings, where results are comparable for both methods. For further discussion of energies see ref 39.

3.2. Condensed Phase Calculations: Liquid. In the following we will use the quantum chemically obtained cluster energies and

Table 2. Optimized QCE Parameters (a_{mf}/b_{xv}) and Error Norm (in mL) of the Different Methods Employed in This Study[a]

	PO			CSO			
method	a_{mf}	b_{xv}	$\|\|\Delta V\|\|$	a_{mf}	b_{xv}	$\|\|\Delta V\|\|$	cluster
PBE/TZVP	0.0253	1.361	0.226	0.0253	1.361	0.226	1, R4, R6a, R6b, R8a
B−P86/TZVP	0.0239	1.372	0.246	0.0238	1.370	0.240	1, C6, R6a, R6b, R8a
MP2/TZVP	0.0672	1.663	3.888	0.0671	1.663	3.886	1, R3, C3, R4, C6, R6a, R6b, R8a
MP2/QZVP	0.0349	1.495	2.280	0.0346	1.492	2.240	1, R3, C3, R4, R6a, R6b, R8a
MP2/QZVP*	0.0348	1.494	2.265	0.0344	1.488	2.224	1, C3, R4, R6a, R6b, R8a
MP2/CBS	0.0255	1.357	0.261	0.0253	1.354	0.254	1, R3, R6a, R6b, R8a
CCSD(T)/CBS	0.0256	1.359	0.265	0.0253	1.354	0.250	1, R6a, R6b, R8a

[a] First block: parameter optimization (PO), and second block: cluster set optimization (CSO). Stepsize in PO $a_{mf} = 0.0001$ and $b_{xv} = 0.001$. Population threshold for CSO 2%.

harmonic frequencies from ref 39 in order to calculate thermodynamic data of the condensed phase. In order to compare the different levels of electronic structure theory, the smaller clusters 1, C2, C3, C6, R3, R4, R6a, R6b, and R8a are considered only, and the R8b, C10, C12, and R_26 clusters are neglected within the first part and will be taken into account in the latter part of this article. Furthermore, to gain insight into the performance of the electronic structure methods, we first apply the quantum cluster equilibrium theory without adjusting the parameters. Thus, the next section shows the obtained isobars from the QCE$^{(0)}$ model.

3.2.1. Evaluation of Methodology: QCE$^{(0)}$. In this section we will only show the isobars calculated from applying $a_{mf} = 0$ and $b_{xv} = 1$, i.e., the QCE$^{(0)}$ model. Thus, there is no interaction between clusters, and the cluster volume is taken into account as the unscaled van der Waals estimate. From the behavior of the obtained isobars we can estimate the influence of the electronic structure method applied, see Figure 2. The orange curves show the DFT results, the blue ones mark MP2 values, and in green we give the CCSD(T) data. All curves show a phase transition which is quite fascinating, keeping in mind that all input stems from static quantum chemical calculations of isolated particles. By setting the QCE parameters to 0 and 1, respectively, a cluster gas is represented. The phase transition as obtained by the DFT methods occurs at higher temperatures than measured by experiment. The calculated volumes are too small which can be explained in terms of "overbinding" as indicated in Table 1. Concerning MP2 values in combination with Ahlrichs basis sets, we observe an opposite trend: At the triple-ζ basis set the temperature of the phase transition is observed to be smaller than measured by experiment. In this case too large volumes indicate "underbinding". This is reduced with increasing basis sets. The phase transition temperature at the complete basis set limit (MP2 and CCSD(T)) is found to be reliable. It is clear that this observation has an impact on the condensed phase. The question is to what extend the QCE parameters can compensate these shortcomings of some of the electronic structure methods when they are optimized.

There is one other aspect worth mentioning. MP2/QZVP*, MP2/CBS, and CCSD(T)/CBS all rely on the same harmonic frequencies and geometries. Therefore, the influence of the accurate calculation of the energy is clearly recognizable. Both curves obtained at the CBS are based on very sophisticated energetics, see ref 39, which thereby can be identified as a necessary prerequisite for an accurate prediction of the phase transition point in the frame of the QCE$^{(0)}$ approach.

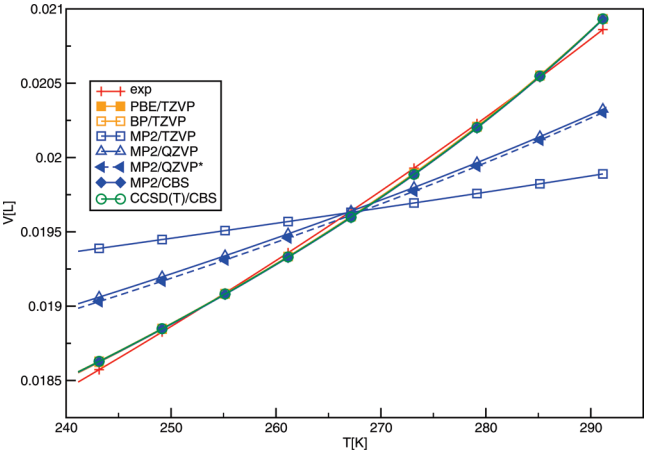

Figure 3. Liquid phase isobars from different quantum chemical methods by adjusting the two parameters a_{mf} and b_{xv}.

3.2.2. Liquid Phase: Isobars and Thermal Expansion Coefficient. We now turn to the optimized QCE model in the liquid phase, i.e., to those calculations in which we adjusted the a_{mf} and b_{xv} values in order to describe the real liquid. Table 2 shows the optimized parameters (PO) a_{mf} and b_{xv} together with the appropriate error norm $\|\Delta V\|$ as well as the result of the cluster set optimization (CSO) with regard to the experimental volume for each method applied.

Table 2 shows that overbinding as observed in case of the DFT calculations can be compensated by optimizing QCE parameters, as here the obtained error norms are comparable to those of the post-Hartree−Fock methods at the complete basis set limit. The MP2 values combined with Ahlrichs basis sets in contrast show deviations which are larger by factor 10. In order to compensate the smaller interaction energies the MP2/TZVP combination provides a larger meanfield parameter a_{mf} and free volume correction b_{xv}. Thus, one can assume that underbinding intracluster energies demand to be balanced by larger intercluster interactions in order to reproduce liquid phase behavior. However, the compensation of the underbinding in terms of the meanfield contribution is not as accurate as the overbinding correction for DFT, as can be seen in the large $\|\Delta V\|$ values obtained for the finite basis set MP2 methods. As a verification, we also adjust a QCE calculation to PBE/TZVP energies and MP2/QZVP* frequencies and geometries. The obtained values are $a_{mf} = 0.0246$, $b_{xv} = 1.3680$, and $\|\Delta V\| = 0.236$. Thus overbinding can easily be corrected which is reflected in the smaller

dx.doi.org/10.1021/ct200074c |J. Chem. Theory Comput. 2011, 7, 868–875

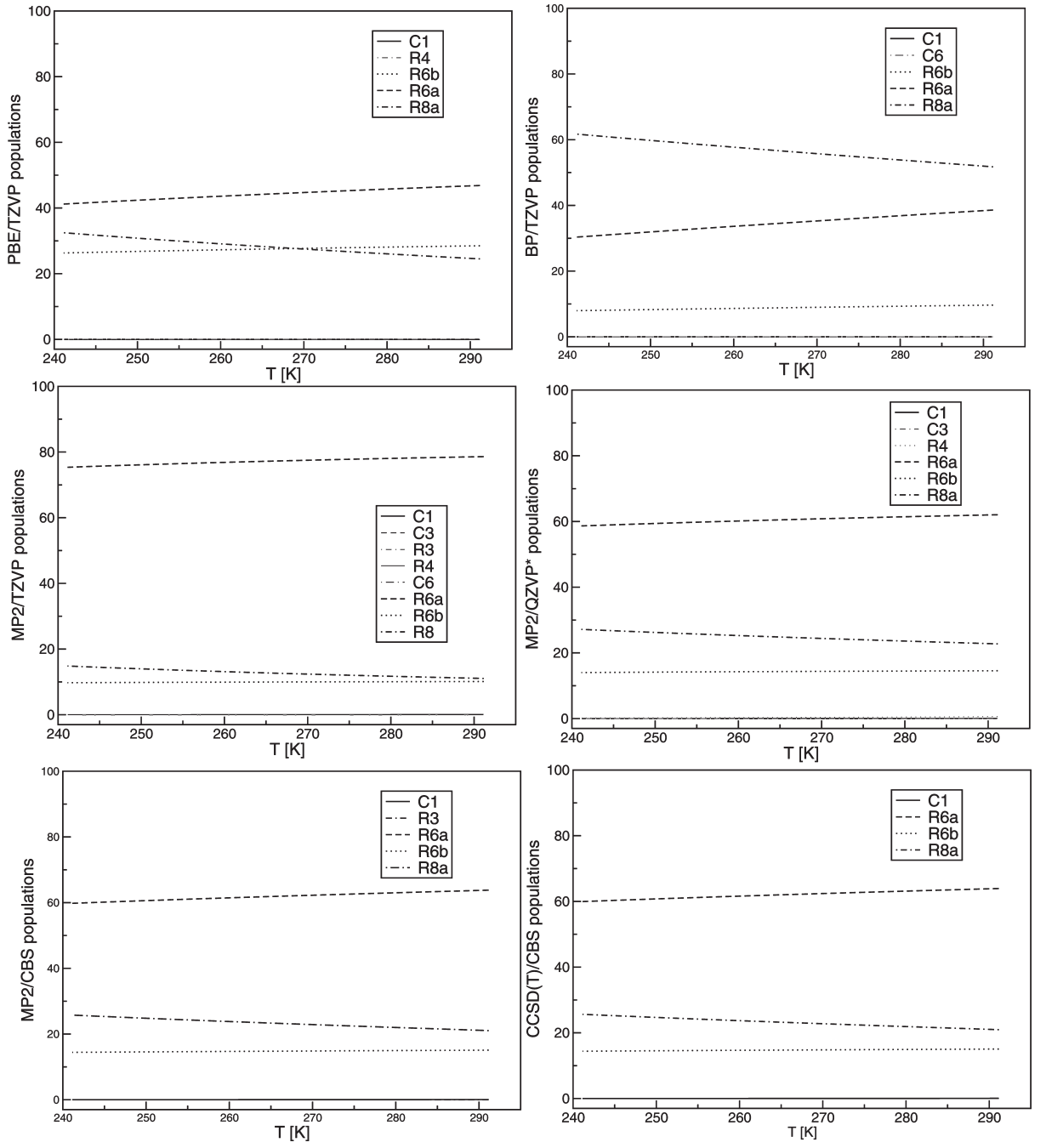

Figure 4. Populations for the different electronic structure methods as obtained from the CSO QCE calculations.

a_{mf} value compared to the pure MP2/QZVP* or MP2/CBS or CCSD(T)/CBS calculations.

Previously, we found that optimizing the cluster set, i.e., excluding some clusters can lead to tremendously improved results thus addressing a destabilizing nature to some clusters.[19] This does not apply to HF, where we found only minor differences leading to improved $||\Delta V||$ as small as 0.01 mL. However, one important result of the CSO procedure is that the six- and eight-membered ring structures are selected independent of the level of theory and the basis set applied, which will be discussed later.

The isobars from the above-discussed PO calculations are depicted in Figure 3. As observed already from Table 2, PBE/TZVP, B−P86/TZVP, MP2/CBS, and CCSD(T)/CBS show excellent agreement with experiment, while the other MP2 values are much more departing from experiment. The large basis set dependency for MP2 is also apparent from Figure 3; compare blue curves with different symbols. These results also show that in a QCE calculation the parameter optimization is unable to account for all deficiencies of the electronic structure methods. While overbinding can be compensated, even slight underbinding is not correctable by a sophisticated choice of parameters.

In order to learn about the topology of liquid phase structures we also show the populations as obtained by the cluster set optimization in Figure 4.

Independent of the methodology, only the ring clusters containing six and eight monomer units contribute significantly. For all

methods the R6a population increases with increasing temperature, and we observe the highest individual cluster population for the R6a cluster for all methods except for the B−P86/TZVP approach. The cluster R8a also contributes significantly, and its population decreases for all methods with increasing temperature. It is clear from simple rules of thumb that the more hydrogen bonds are formed, the more stable ring clusters are in the gas phase. However, the larger the ring clusters are the more they resemble chain clusters which was stated by Hammes-Schiffer and co-workers.[41] Therefore, it is reasonable that the larger clusters show higher populations than the smaller clusters which will be further investigated in Section 3.2.3.

Figure 5 shows the temperature dependency of the thermal expansion coefficient. Please note that this quantity is calculated according to

$$\alpha = \frac{1}{V}\left(\frac{\partial V}{\partial T}\right) \qquad (12)$$

and, thus, does not directly depend on the partition function but on the volume and its first derivative. This is the reason why those methods able to accurately reproduce the phase volume yield values for the thermal expansion coefficient are in good agreement with experimental data.

3.2.3. Extending the Motifs: Larger Chain Clusters. Turning now to QCE calculations with larger clusters, we show the results of the B−P86/TZVP data including the R8b, C12, and $R_2$6 and of the MP2/TZVP input data including the R8b, C10, C12, and $R_2$6 clusters, see Table 3. The choice of these two methods is related to the fact that for other electronic structure methods, the C10 and C12 are no minimum structures. The a_{mf} value is decreased for the B-P86/TZVP input data and increased in case of the MP2/TZVP. However, the accuracy is not improved but slightly worse than for the smaller cluster set.

This is also the case if instead of a PO calculation a CSO calculation is chosen, see Table 3. The results are slightly worse than for the CSO with the smaller cluster set. Regarding the population, almost nothing changed compared to calculations applying the smaller cluster set, as the dominant species still consist of six-membered and eight-membered rings (populations not shown here).

3.3. Phase Transition: Isobars. In this section we consider the results up to the boiling point with optimized parameter values from a new PO calculation. In this case the reference isobar only consists of two values at the temperatures 292.15 and 293.15 K, the highest temperature in the liquid phase and the lowest

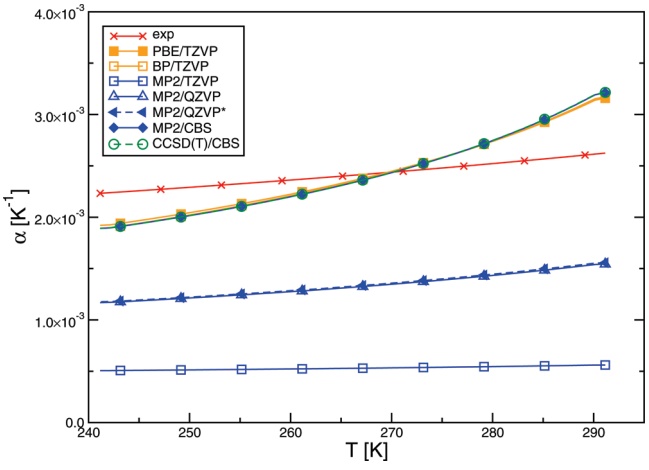

Figure 5. Thermal expansion coefficient α for different quantum chemical methods as obtained from the CSO QCE calculations. Experimental data from ref 42.

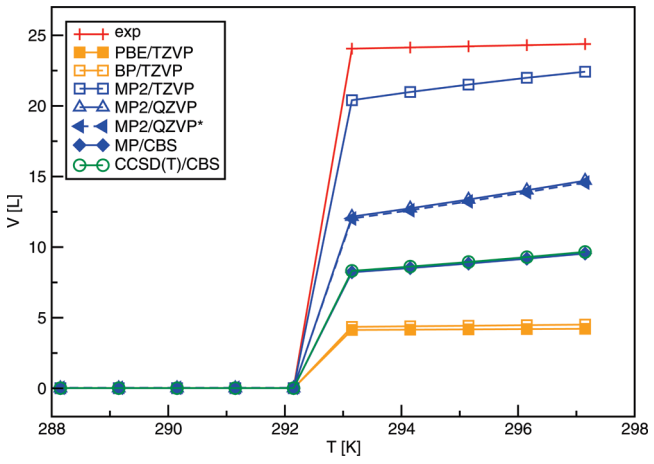

Figure 6. Liquid−gas phase transition isobars from different quantum chemical methods by optimizing the two parameters a_{mf} and b_{xv} for the phase transition.

Table 4. Optimized QCE Parameters (a_{mf}/b_{xv}) and Error Norm (in L) of the Different Methods Employed in This Study[a]

	PO		
method	a_{mf}	b_{xv}	$\|\|\Delta V\|\|$
PBE/TZVP	0.0088	1.009	19.920
B−P86/TZVP	0.0092	1.005	19.698
MP2/TZVP	0.0419	1.001	3.650
MP2/QZVP	0.0283	1.153	11.900
MP2/QZVP*	0.0754	3.103	12.033
MP2/CBS	0.0169	1.005	15.834
CCSD(T)/CBS	0.0171	1.005	15.733

[a] Stepsize in PO a_{mf} = 0.0001 and b_{xv} = 0.001.

Table 3. Optimized QCE Parameters (a_{mf}/b_{xv}) and Error Norm (in mL) of the Different Methods Employed in This Study[a]

	PO			CSO			
method	a_{mf}	b_{xv}	$\|\|\Delta V\|\|$	a_{mf}	b_{xv}	$\|\|\Delta V\|\|$	cluster
B-P86/TZVP	0.0225	1.366	0.255	0.0225	1.366	0.255	C1, R4, R6a, R6b, C6, R8a, R8b
MP2/TZVP	0.0674	1.668	3.904	0.0672	1.667	3.889	C1, C3, R3, R4, C6, R6a, R6b, R8a, R8b, $R_2$6

[a] First block: parameter optimization (PO), and second block: cluster set optimization (CSO). Stepsize in PO a_{mf} = 0.0001 and b_{xv} = 0.001. Population threshold for CSO 2%.

dx.doi.org/10.1021/ct200074c |J. Chem. Theory Comput. 2011, 7, 868–875

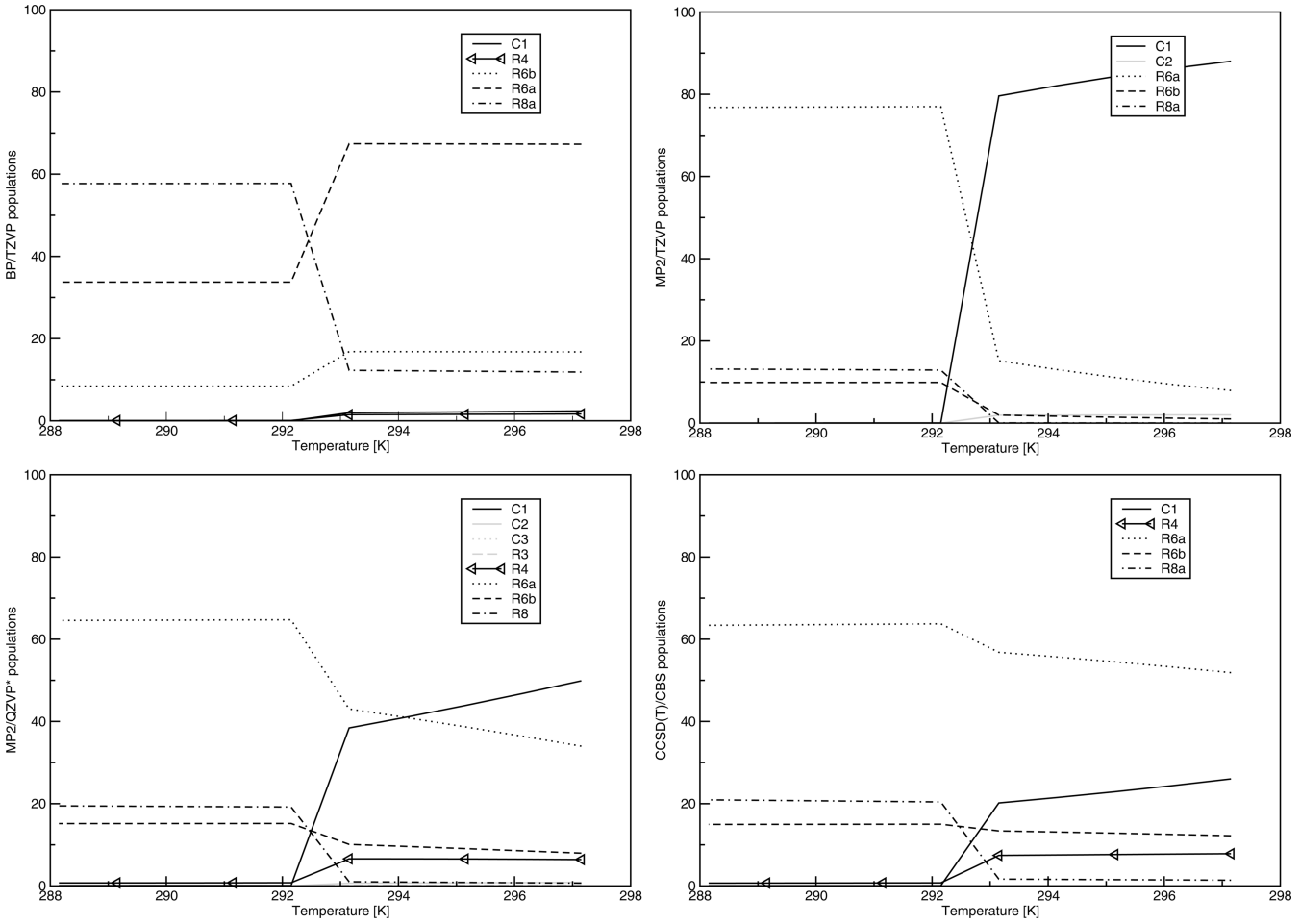

Figure 7. Liquid−gas phase transition populations for different quantum chemical methods by optimizing the two parameters a_{mf} and b_{xv} for the phase transition.

temperature in the gaseous phase, respectively. Of course, the selection of adjustment temperatures might be enhanced, however, for a first indication of the performance at the boiling point, this two-point fit is sufficient enough. The corresponding results are shown in Figure 6, and the obtained parameters from this two-point adjustment are given in Table 4. Please note that in Table 4 the squared deviations are given in L and not in mL.

The difficulty in reproducing the phase transition is apparent by the fact that (in the gas phase) now different error cancellations play a role, and therefore different quantum chemical methods perform best contrary to the behavior in the bulk liquid phase. From Figure 6 and Table 4 we recognize that MP2/TZVP with its smallest interaction energies yields the highest accuracy. While DFT performs worst, the numbers from the best electronic structure method lie in between. Interestingly the excluded volume is almost not scaled (b_{xv} = 1) in order to account for the gas phase. Please note that we did not allow this parameter to shrink beyond 1.0 in this particular optimization.

In Figure 7 we show the cluster populations as they occur in our QCE calculations for four selected electronic structure methods. Please note that the neglected electronic structure cases give similar results to those methods which they match regarding the isobars. Obviously, the good performance of MP2/TZVP is due to the population of the monomer species, and the bad performance of DFT is due to the missing occupancy of the monomer species. Interestingly, in the region of the boiling point the vapor phase consists still of a variety of different clusters, for example both six-membered rings and even the eight-membered rings contribute to some extent. McGrath et al. have recently investigated the vapor of HF from ab initio Monte Carlo simulations.[43] Although the authors worked at much higher temperature, they found the prominence of monomeric species as well, next to some populations of a six-membered ring.[43]

4. CONCLUSION

We presented the first quantum cluster equilibrium (QCE) calculations for the liquid phase based on highly accurate CCSD(T) computations of the underlying cluster structures. Furthermore the coupled cluster method and the second order Møller−Plesset perturbation theory (MP2) were applied at the complete basis set limit. In order to compare the outcome of the QCE calculations, we also applied other electronic structure data as input. These were obtained from density functional theory (DFT), namely B-P86/TZVP and PBE/TZVP, and from the MP2 method in combination with different Ahlrichs basis sets. The interaction energies are such that DFT provides strongest hydrogen bonds, MP2/TZVP weakest interaction energies, and the CCSD(T) and MP2 at the complete basis set limit values in between in high agreement with experimental data. The QCE$^{(0)}$ calculations were carried out without taking additional interaction or volume scaling into account. For all

electronic structure methods this led to isobars with boiling points more or less away from experimental values. While the DFT methods provided too small volumes and therefore too large densities showing the well-known behavior of overbinding, the MP2/TZVP values were slightly too large, and the data obtained from the complete basis set limit calculations were very close to the experimental boiling point.

In order to model a realistic liquid, the two parameters were adjusted, and it was found that DFT and the correlated electronic structure methods at the complete basis set limit agreed best with the experimental isobar. For the MP2 combinations with the smaller basis sets no such agreement with experiment could be achieved despite the fact that two parameters are used. From the populations we learned that an important topology lies in the six- and eight-ring clusters. While the former is increasing with higher temperature, the latter is decreasing. Inclusion of larger chain clusters did not change the picture significantly, still the six- and eight-membered rings played the dominant role in order to reproduce the liquid phase.

We also provided a first estimate of the performance at the phase transition. Here different error cancellations played a role. For example, the weakest bound structures (MP2/TZVP) were now leading to the best agreement with the experimental curve, because the gas phase can be modeled more accurately by those methods which yield less stable hydrogen bonds. In all cases we found a variety of clusters with small populations at the vapor phase in agreement with literature.[43] In further studies we will examine these issues in more detail and investigate other cluster structures.

To summarize, we can say that in order to arrive at a consistent multiscale condensed phase description based on the resolution of the electronic structure, the accurate treatment of the underlying electronic structure problem is necessary. However, if one is only interested in good agreement with experiment, a pragmatic point of view in which error cancellation is taken into account is possible if overbound cluster energies are used for the liquid phase and underbound energies for the gas phase.

AUTHOR INFORMATION

Corresponding Author

*E-mail: bkirchner@uni-leipzig.de.

Present Addresses

[§]Lehrstuhl für Anorganische Chemie 2, Organometallics and Materials Chemistry, Ruhr-Universität Bochum, Universitätsstrasse 150, D-44780 Bochum.

ACKNOWLEDGMENT

This work was supported by the DFG, in particular by the projects KI-768/4-1 and KI-768/4-2 from the ERA-chemistry, KI-768/5-1, and KI-768/5-2 SPP-IL program and the KI-768/7-1 project. Computer time from the RZ Leipzig is gratefully acknowledged.

REFERENCES

(1) Fielding, H.; Lee, B. *Chem. Br.* **1978**, *14*, 173.
(2) O'Donnell, T. A. *Superacids and Acidic Melts as Inorganic Chemical Reaction Media*; VCH Publishers: New York, 1992; pp 41 − 51.
(3) Olah, G. A. *Angew. Chem., Int. Ed. Engl.* **1995**, *34*, 1393–1405.
(4) McLain, S. E.; Benmore, C. J.; Siewenie, J. E.; Urquidi, J.; Turner, J. F. C. *Angew. Chem., Int. Ed. Engl.* **2004**, *43*, 1952–1955.
(5) Visco, D. P.; Kofke, D. A. *Fluid Phase Equilib.* **1999**, *158*, 37–47.
(6) Weinhold, F. *J. Chem. Phys.* **1998**, *109*, 367–372.
(7) Weinhold, F. *J. Chem. Phys.* **1998**, *109*, 373–384.
(8) Kirchner, B. *J. Chem. Phys.* **2005**, *123*, 204116.
(9) Kirchner, B. *Phys. Rep.* **2007**, *440*, 1–111.
(10) Ludwig, R.; Weinhold, F. *J. Chem. Phys.* **1999**, *110*, 508–515.
(11) Ludwig, R.; Weinhold, F.; Farrar, T. C. *J. Chem. Phys.* **1995**, *103*, 3636–3642.
(12) Matisz, G.; Fabian, W. M. F.; Kelterer, A.-M.; Kunsagi-Mate, S. *J. Mol. Struct. (THEOCHEM)* **2010**, *956*, 103–109.
(13) Kirchner, B.; Spickermann, C.; Lehmann, S. B. C.; Perlt, E.; Langner, J.; von Domaros, M.; Reuther, P.; Uhlig, F.; Kohagen, M.; Brüssel, M. *J. Comp. Phys. Comm.* **2011**submitted.
(14) Borowski, P.; Jaroniec, J.; Janowski, T.; Woliński, K. *Mol. Phys.* **2003**, *101*, 1413–1421.
(15) Wendt, M. A.; Weinhold, F.; Farrar, T. C. *J. Chem. Phys.* **1998**, *109*, 5945–5947.
(16) Ludwig, R.; Behler, J.; Klink, B.; Weinhold, F. *Angew. Chem., Int. Ed. Engl.* **2002**, *41*, 3199–3202.
(17) Song, H.-J.; Xiao, H.-M.; Dong, H.-S.; Huang, Y.-G. *J. Mol. Struct. (THEOCHEM)* **2006**, *767*, 67–73.
(18) Spickermann, C.; Lehmann, S. B. C.; Kirchner, B. *J. Chem. Phys.* **2008**, *128*, 244506.
(19) Lehmann, S. B. C.; Spickermann, C.; Kirchner, B. *J. Chem. Theory Comput.* **2009**, *5*, 1640–1649.
(20) Lehmann, S. B. C.; Spickermann, C.; Kirchner, B. *J. Chem. Theory Comput.* **2009**, *5*, 1650–1656.
(21) Lenz, A.; Ojamae, L. *J. Chem. Phys.* **2009**, *131*, 134302.
(22) Maerker, C.; v. R. Schleyer, P.; Liedl, K. R.; Ha, T. K.; Quack, M.; Suhm, M. A. *J. Comput. Chem.* **1997**, *18*, 1695–1719.
(23) Quack, M.; Stohner, J.; Suhm, M. A. *J. Mol. Struct.* **2001**, *599*, 381–425.
(24) Buth, C.; Paulus, B. *Phys. Rev. B* **2006**, *74*, 045122.
(25) Wierzchowski, S. J.; Fang, Z. H.; Kofke, D. A.; Tilson, J. L. *Mol. Phys.* **2006**, *104*, 503–513.
(26) Li, J. *J. Theor. Comp. Chem.* **2006**, *5*, 187–196.
(27) Rincòn, L.; Almeida, R.; Garca-Aldea, D.; Diez y Riega, H. *J. Chem. Phys.* **2001**, *114*, 5552–5561.
(28) Guedes, R. C.; do Couto, P. C.; Cabral, B. J. C. *J. Chem. Phys.* **2003**, *118*, 1272–1281.
(29) Sangster, M. *J. Phys. Chem. Solids* **1974**, *35*, 195–200.
(30) Klein, M. L.; McDonald, I. R. *J. Chem. Phys.* **1979**, *71*, 298–308.
(31) Röthlisberger, U.; Parrinello, M. *J. Chem. Phys.* **1997**, *106*, 4658–4664.
(32) Jedlovszky, P.; Vallauri, R. *J. Chem. Phys.* **1997**, *107*, 10166–10176.
(33) Valle, R. G. D.; Gazzillo, D. *Phys. Rev. B* **1999**, *59*, 13699–13706.
(34) Kreitmeir, M.; Bertagnolli, H.; Mortensen, J. J.; Parrinello, M. *J. Chem. Phys.* **2003**, *118*, 3639–3645.
(35) Pfleiderer, T.; Waldner, I.; Bertagnolli, H.; Tölheide, K.; Fischer, H. E. *J. Chem. Phys.* **2000**, *113*, 3690–3696.
(36) Deraman, M.; Dore, J.; Powles, J.; Holloway, J. H.; Chieux, P. *Mol. Phys.* **1985**, *55*, 1351–1367.
(37) Huber, H.; Dyson, A. J.; Kirchner, B. *Chem. Soc. Rev.* **1999**, *28*, 121–133.
(38) Kirchner, B.; Spickermann, C. *PEACEMAKER*, v1.4; University of Bonn, Institute of Physical and Theoretical Chemistry, University of Leipzig, Wilhelm-Ostwald Institute of Physical and Theoretical Chemistry Bonn: Leipzig, Germany, 2008; http://www.uni-leipzig.de/~quant/index.html/ and http://www.uni-leipzig.de/~peacemaker/. Both accessed March 1, 2011.
(39) Friedrich, J.; Perlt, E.; Roatsch, M.; Spickermann, C.; Kirchner, B. *J. Chem. Theory Comput.* **2011**; doi: 10.1021/ct100131c.
(40) Halkier, A.; Klopper, W.; Helgaker, T.; Jørgensen, P.; Taylor, P. R. *J. Chem. Phys.* **1999**, *111*, 9157.
(41) Swalina, C.; Wang, Q.; Chakraborty, A.; Hammes-Schiffer, S. *J. Phys. Chem. A* **2007**, *111*, 2206–2212.
(42) Yaws, C. L. *Chemical Properties Handbook*; McGraw-Hill: New York, 1999; p 639.
(43) McGrath, M. J.; Ghogomu, J. N.; Mundy, C. J.; Kuo, I.-F. W.; Siepmann, J. I. *Phys. Chem. Chem. Phys.* **2010**, *12*, 7678–7687.